Journal of Alloys and Compounds, 207/208 (1994) 120–127
JALCOM 3027

Investigation of charge transfer $O^{2-} \rightarrow Ln^{3+}$ and $F^- \rightarrow Ln^{3+}$ in LaF_3:(Ln^{3+}, O^{2-}) and YF_3:(Ln^{3+},O^{2-}) systems

I. Gérard[a,b], J.C. Krupa[a], E. Simoni[a] and P. Martin[c]
[a]*Institut de Physique Nucléaire - Radiochimie, Bât. 100, 91406 Orsay Cedex (France)*
[b]*Thomson TDO, BP 320, 38523 St Egrève Cedex (France)*
[c]*LURE, Bât. 209 C, 91405 Orsay Cedex (France)*

Abstract

Excitation spectra of the visible luminescence of Eu^{3+}, Dy^{3+}, Er^{3+} ions doped into two fluoride matrices, LaF_3 and YF_3, holding some traces of O^{2-} ions were recorded in the UV and VUV range. Charge transfer bands $O^{2-} \rightarrow Ln^{3+}$ ($Ln^{3+} = Eu^{3+}$, Dy^{3+}, Er^{3+}) and $F^- \rightarrow Eu^{3+}$ appear clearly on excitation spectra recorded at low temperature. Using the experimental data and Jorgensen's theoretical developments, it becomes possible to predict the energy of charge transfer $O^{2-} \rightarrow Ln^{3+}$ and $F^- \rightarrow Ln^{3+}$ for all the trivalent ions of the lanthanide series. The time-dependent theory was used to simulate the CT absorption profile.

1. Introduction

Since Jørgensen [1,2] assigned the broad and strong absorption band in the spectra of the trivalent lanthanides to charge transfer transition, many studies dealing with solutions, and extended to solids, have followed this particular investigation [3,4].

A charge transfer (CT) from the ligand to the central ion means in molecular orbital (MO) theory, electronic transitions from states having essentially ligand character to states located essentially on the central ion. The CT transitions are allowed as pure electronic transitions and are translated on spectra by broad bands with high intensity.

The energy of the charge transfer bands depends on many factors. For example, Hoefdraad [5] showed, in the case of Eu^{3+}, that the coordination number is a determining factor; in octahedral VI coordination, the CT band does not depend markedly on the host lattice, but in cubic VIII and XII coordinations, the CT band varies proportionally to the Eu–L (L = ligand) distance and shifts to lower energy when the bond length increases. This can be explained if we consider the ligand stabilization by the surrounding positive ions. Thus, when the cation has a smaller radius and carries a higher charge density, the ligand is more stabilized and therefore the Eu–L distance becomes smaller. In other words, it is then necessary to spend more energy to remove an electron from the ligand. With the same considerations, it is easy to predict the dependency of the CT band with the nature of the ligand. This is illustrated by the changes in band energy from chloride to iodide in a variety of halide complex systems [3].

Jørgensen [6] showed that this variation correlates well the Pauling electronegativities and he defined a new concept of optical electronegativity χ_{opt} which connects the CT band energy to the change in χ_{opt} between halogens. This concept is very useful to predict the energy of the CT band in different environments [7,8].

The last consideration on the CT energy band position rests on the nature of the Ln^{3+} ions. Barnes and Day [9] showed that the band energy increases linearly with M^{3+}/M^{2+} redox potential. The CT process corresponds to a reduction; it means that the Ln^{3+} ion gains one electron. If we neglect the energy loss to relax the Ln^{3+} ion, the comparison of the energies of CT bands with the second ionization potential, $I_{Ln}{}^{2+}$, versus the number of 4f electrons leads to a good correlation [10].

Experimental investigation of these features was generally limited to the UV or visible energy range. Synchrotron radiation as a VUV light source allows us to extend the excitation energy range and to bring new data on energy of CT bands, especially those dealing with F^- and O^{2-} ($F^- \rightarrow Ln^{3+}$ and $O^{2-} \rightarrow Ln^{3+}$) arising in the VUV domain.

The charge transfer $L^- \rightarrow Ln^{3+}$ ($L^- = F^-$ or O^{2-}) corresponds to electron delocalization from the highest filled molecular orbitals 2p of the ligand to the partly filled 4f shell of the Ln^{3+} ion. These opposite parity

SSDI 0925-8388(93)03027-G

transitions are allowed, and appear on the spectra as broad and intense bands.

The spectral position of the CT band is connected with the degree of filling of the 4f shell, and is then closely related to the electroaffinity of the lanthanide ion. For example, the charge transfer from the ligand to the metal ion requires less energy to promote one electron to complete a half filled or a filled stable 4f shell. This is the case for trivalent lanthanides, Eu^{3+} ($4f^6$) and Yb^{3+} ($4f^{13}$) ions, respectively. Then the CT band $L^- \rightarrow Eu^{3+}$ or $L^- \rightarrow Yb^{3+}$ should be observed at lower energy than for the other Ln^{3+} ions in the series. In the case of fluoride ligands, the high electronegativity of fluorine F^- will shift charge transfer $F^- \rightarrow Ln^{3+}$ in the VUV energy range except for the Eu^{3+} ion ($4f^6$), where CT arises at rather low energy.

In the case of oxygen ligands, for the same reason, CT band $O^{2-} \rightarrow Eu^{3+}$ appears generally at low energy, in the UV range [11]. For the other Ln^{3+} ions, such as Er^{3+} or Dy^{3+}, CT from oxygen ligand arises at rather high energy and bands are generally hidden by the host lattice absorptions

For this reason, we have chosen to work in fluoride matrices which are inorganic insulators well known for their intrinsic transparency in the near IR, visible, UV and VUV range, up to 9–12 eV. This property is due to the high value of the energy gap between the conduction and the valence bands in these materials: 11.5 eV and 12 eV in LaF_3 [12] and YF_3 [13], respectively.

When trivalent rare earth ions are substituted for La^{3+} and Y^{3+} in these fluorides, two types of photon absorption process can take place in the UV range below 10–11 eV:

(1) Electron transfer from the L^- anion ($L^- = F^-$, O^{2-}) to the Ln^{3+} rare earth ions which occurs generally at high energy and have not been observed in the case of $L^- = F^-$ except for Eu^{3+} and Yb^{3+}.

(2) Inter-configurational transitions $4f^n \rightarrow 4f^{n-1}5d$ in Ln^{3+} ions which occur in the VUV energy range below 10 eV [12,14,15]. This energy shifts towards low energy for Ce^{3+} and Tb^{3+} which easily lose one electron to reach the more stable configuration, $4f^0$ and $4f^7$, respectively.

CT and the f–d transitions are both opposite parity transitions, and are allowed transitions with a large vibronic character. However, f–d transitions are generally weaker and if they are superposed on the CT band, they cannot be distinguished.

In the present work, experimental data and Jorgensen's theoretical developments, were used to predict the energy of the $O^{2-} \rightarrow Ln^{3+}$ and $F^- \rightarrow Ln^{3+}$ charge transfer for all the trivalent ions of the lanthanide series. The time-dependent theory was used to simulate the CT absorption profile

2. Technical procedures

Excitation spectra of the visible fluorescence of the doped fluoride systems were recorded from 50 to 350 nm (25–3.5 eV) using the synchrotron radiation from the positron storage ring "SUPERACO" at the "Laboratoire pour l'Utilisation du Rayonnement Electromagnétique (LURE)" at Orsay. The synchrotron radiation light was dispersed through a 3-m computer-driven monochromator maintained at 10^{-9} Torr. The large energy range was scanned using a 300 g mm^{-1} grating blazed at 63 nm offering a 1 nm per mm dispersion. The beam spot on the sample showed an area of approximately 3 mm^2. The VUV incident photon intensity and its temporal variation was determined by using the photoelectron current produced on a gold grid bombarded by 20.7 eV (60 nm) photons with a cross-section yield of 0.12.

A fraction of the visible light emitted from the samples was guided by a quartz rod to a Hamamatsu R928 photomultiplier window. Bandpass glass filters matched to the emission peaks of the phosphors were placed between the window and the rod to eliminate second order radiation and diffuse or specular reflections in VUV and UV range. The output signal voltage was converted into frequency in order to be stored in the computer memory versus excitation wavelength in the excitation range.

The spectral characteristics of the beam and the monochromator transmission were taken into account by recording powdered sodium salicylate spectrum in the same conditions as for the sample. Sodium salicylate, with emission centered at 443 nm, is assumed to have a constant quantum efficiency over the whole UV and VUV excitation range [16]. The excitation spectra presented in this paper were obtained by dividing the sample spectrum values by the corresponding value for sodium salicylate.

LaF_3:(Ln^{3+},O^{2-}) and YF_3:(Ln^{3+},O^{2-}) powdered samples were prepared by heating at 1100 °C the mixture of commercially available high purity LaF_3 and YF_3 materials doped with 1% in weight of rare earth fluorides such as EuF_3, DyF_3, ErF_3. The mixture was introduced in a platinum crucible placed in a quartz tube. The heating procedure was performed under argon circulation to avoid the formation of oxyfluoride. This procedure permits a small amount of oxygen contamination, due to H_2O hydration molecules of the initial chemicals, which plays an important role in the de-excitation mechanisms occurring in some of the compounds investigated [13]. The luminescent polycrystalline compounds were pressed into cylindrical depressions set in a copper sample holder which can be cooled up to approximately 10 K by liquid helium circulation.

3. Results

The vacuum-UV excitation spectra of the visible luminescence of LaF_3:(Ln^{3+},O^{2-}) and YF_3:(Ln^{3+},O^{2-}), with $Ln^{3+} = Eu^{3+}$, Dy^{3+} and Er^{3+}, were recorded at different temperatures between 300 K and 10 K.

The relative intensity of the bands observed on the excitation spectra of the visible luminescence reflects the combined efficiencies of two processes: absorption and energy transfer to the $4f^n$ emitting levels of the rare earth ion under consideration.

At low temperature, only a few broad bands, which are attributed to charge transfer transitions, remain on the excitation spectra (Figs. 1–6). According to these experimental data, we can say that the energy transfer probabilities from the $4f^{n-1}5d$ excited states to the $4f^n$ visible levels of Ln^{3+} ions become extremely weak when the temperature is decreasing (except for YF_3:(Dy^{3+},O^{2-})), while energy transfer from the CT state to the $4f^n$ levels still occurs with high efficiency [13]. As a consequence, at low temperature and below 10 eV, the excitation bands connected to the charge transfers appear quite clearly on the excitation spectra of the visible luminescence.

Thus, the broad band observed around 160 nm (7.75 eV) on the excitation spectra of YF_3:(Eu^{3+},O^{2-}) (Fig. 1) and LaF_3:(Eu^{3+},O^{2-}) (Fig. 4) was attributed to the charge transfer $F^- \rightarrow Eu^{3+}$. The CT bands $F^- \rightarrow Dy^{3+}$ and $F^- \rightarrow Er^{3+}$ are expected at higher energy but they do not appear on excitation spectra recorded at low temperature. This can be explained by the absence of energy transfer to the $4f^n$ emitting levels of the rare earth ions.

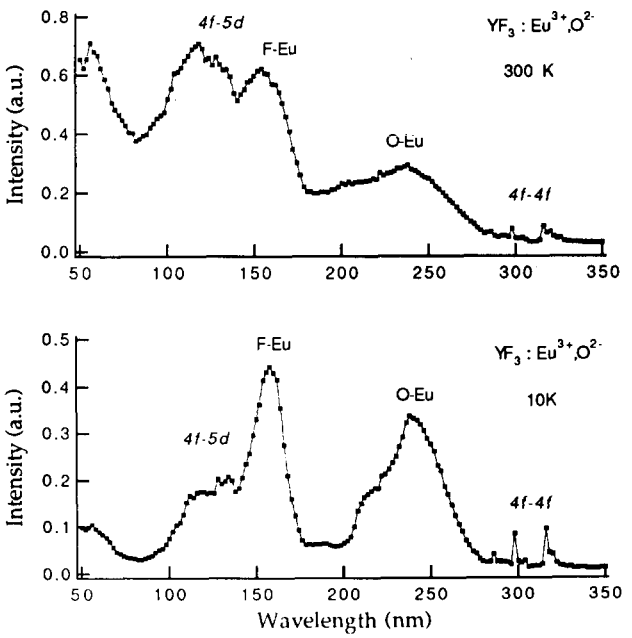

Fig. 1. Vacuum-UV excitation spectra of the visible luminescence recorded at room and at low temperature of YF_3:(Eu^{3+},O^{2-}).

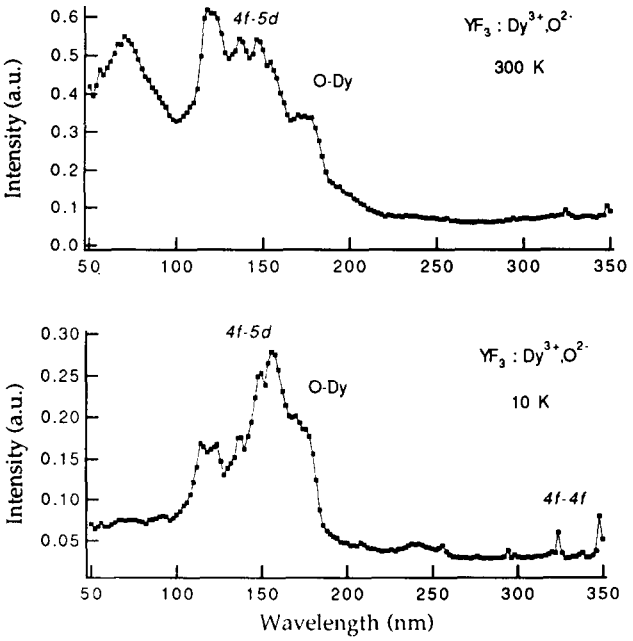

Fig. 2. Vacuum-UV excitation spectra of the visible luminescence recorded at room and at low temperature of YF_3:(Dy^{3+},O^{2-}).

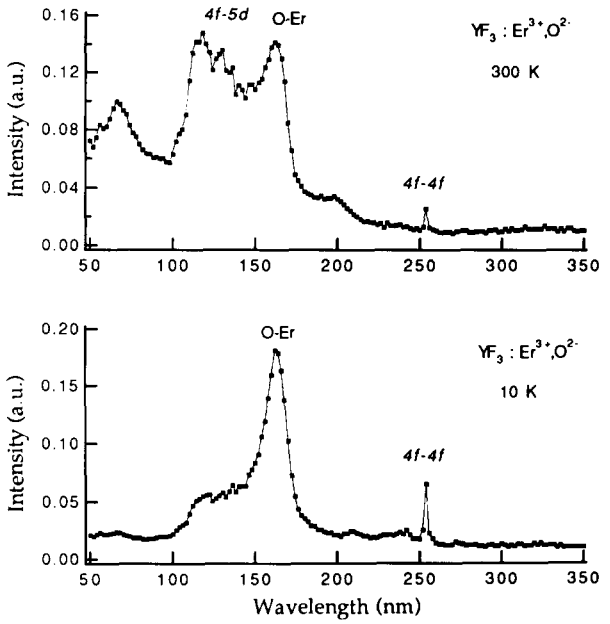

Fig. 3. Vacuum-UV excitation spectra of the visible luminescence recorded at room and at low temperature of YF_3:(Er^{3+},O^{2-}).

The YF_3:(Eu^{3+},O^{2-}) system shows a broad UV band centered around 5 eV (~250 nm) which corresponds to the known $O^{2-} \rightarrow Eu^{3+}$ CT band. Dy^{3+} and Er^{3+} ions have lower electroaffinity than Eu^{3+} and the charge transfers $O^{2-} \rightarrow Dy^{3+}$ and $O^{2-} \rightarrow Er^{3+}$ are expected at higher energy. In oxygen matrices, these two latter mechanisms are generally hidden by interband transitions occurring in the host lattice. In the fluoride

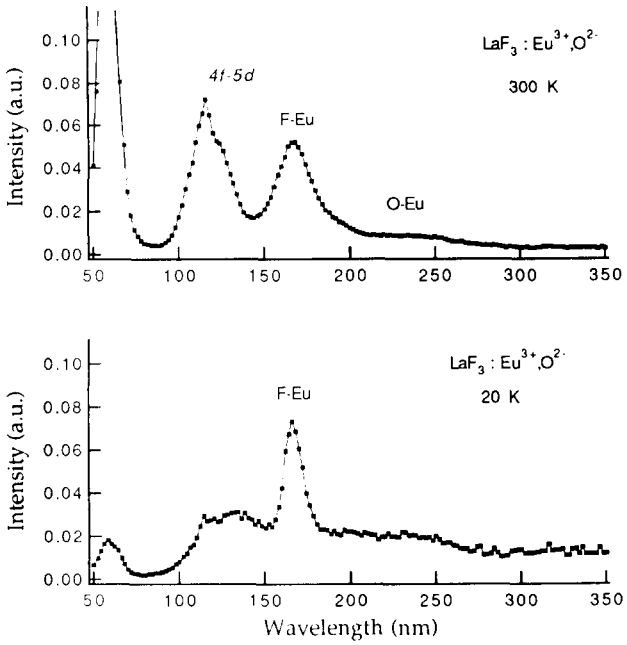

Fig. 4. Vacuum-UV excitation spectra of the visible luminescence recorded at room and at low temperature of LaF_3:(Eu^{3+},O^{2-}).

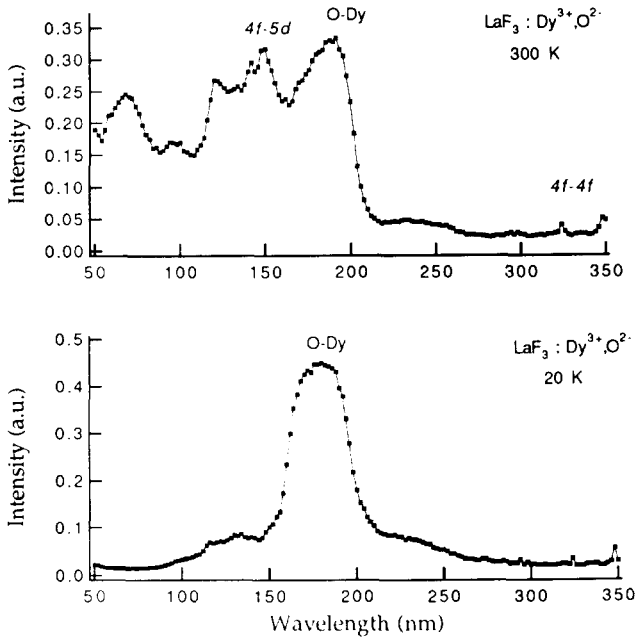

Fig. 5. Vacuum-UV excitation spectra of the visible luminescence recorded at room and at low temperature of LaF_3:(Dy^{3+},O^{2-}).

matrices, YF_3 and LaF_3, the large gap between the valence and conduction bands allows the bands due to CT between oxygen ligand and the metallic central ion to be clearly displayed: $O^{2-} \rightarrow Dy^{3+}$ or $O^{2-} \rightarrow Er^{3+}$. At low temperature, only these bands remain and broad excitation features are observed at approximately 7.5 eV (~165 nm) for YF_3:(Dy^{3+},O^{2-}) and YF_3:(Er^{3+},O^{2-}) (Figs. 2 and 3), and ~7 eV (~180 nm) for

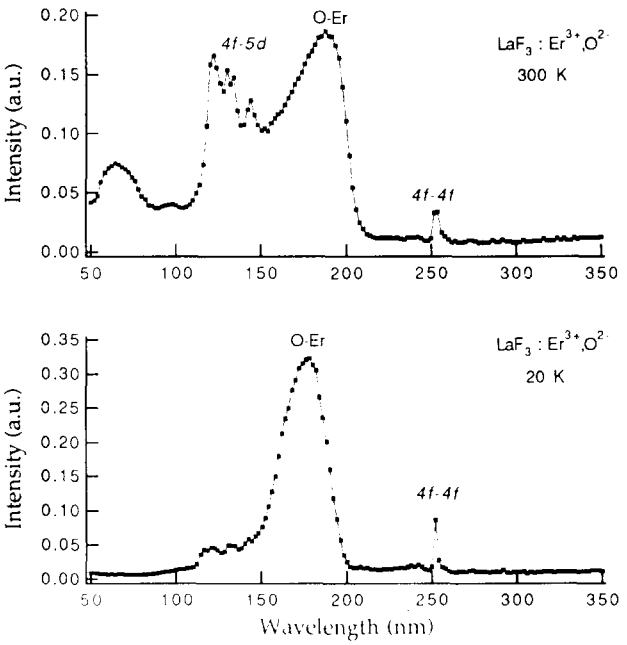

Fig. 6. Vacuum-UV excitation spectra of the visible luminescence recorded at room and at low temperature of LaF_3:(Er^{3+},O^{2-}).

LaF_3:(Dy^{3+},O^{2-}) and LaF_3:(Er^{3+},O^{2-}) (Figs. 5 and 6). These bands are unambiguously connected to the corresponding $O^{2-} \rightarrow Dy^{3+}$ and $O^{2-} \rightarrow Er^{3+}$ charge transfer.

4. Charge transfer $O^{2-} \rightarrow Ln^{3+}$

Jørgensen's refined spin-pairing energy theory [1,2] has been generally found effective for correlation and prediction of energy of charge transfer band in a variety of Ln complexes [17,18].

Jørgensen has formulated the energy change when an electron is added to a f^q configuration as follows:

$$E_{TC} = W - q(E - A) + \frac{9}{104} N(S)E^1 + M(L)E^3 + P(S, L, J)\zeta_{4f} \quad (1)$$

where W corresponds to the energy transfer of an electron from the ligand (2p MO) to the 4f shell of Ln^{3+}, if all electron shieldings were perfect, if there were no repulsions among the f-electrons, and if there were no f-electron spin-orbit or relativistic interactions. $E - A$ reflects the difference between stronger nuclear attraction E and increased interelectronic repulsion A across the 4f shell. $N(S)E^1$ is the difference in spin-pairing energy for the f^q and f^{q+1} configurations. The first order Racah parameter E^1 of inter-f-electron repulsion is assumed to be the same for both the III and IV oxidation states. $M(L)E^3$ reflects the energy differences between terms with S_{max}; the function $M(L)$,

where L is the total electron orbital angular momentum quantum number, represents the difference between the coefficients of the Racah inter-f-electron repulsion parameter, E^3, in the ground electronic state of the III and IV oxidation states, respectively. $P(S,L,J)\zeta_{4f}$ expresses the influence of the spin-orbit coupling.

Values for the functions $N(S)$, $M(L)$ and $P(S,L,J)$ originally determined by Jørgensen are listed in ref. 4 with the corresponding values of q for each lanthanide. The phenomenological parameters E^1, E^3 and ζ_{4f} which are used, were determined by Carnall *et al.* in LaF_3 [19]. These parameters are only slightly dependent on the host lattice and are assumed to be the same for LaF_3:(Ln^{3+},O^{2-}) and YF_3:(Ln^{3+},O^{2-}).

If the combined parameters W and $(E-A)$ are supposed constant along the 4f series, the fitting of energy transfer $O^{2-} \rightarrow Ln^{3+}$ ($Ln^{3+} = Eu^{3+}$, Dy^{3+}, Er^{3+}) using eqn. (1) and experimental data, leads to the following parameter sets for each system:

(1) for YF_3:(Ln^{3+},O^{2-}): $W = 86.6 \times 10^3$ cm^{-1} and $(E-A) = 4 \times 10^3$ cm^{-1}

(2) for LaF_3:(Ln^{3+},O^{2-}): $W = 82.0 \times 10^3$ cm^{-1} and $(E-A) = 4 \times 10^3$ cm^{-1}.

The difference in the W parameter for the two systems reflects the difference in ionic radius between Y^{3+} and La^{3+} ions which induced O^{2-} orbital stabilization more significantly in YF_3 than in LaF_3.

Calculated values and experimental data are in good agreement (Table 1) and allow Jørgensen's eqn. (1) to be applied using the determined parameter sets for all the lanthanide ions in the series and for the two fluorides systems.

Results have been plotted in Fig. 7 where the variation of the charge transfer energy versus the number of 4f electrons follows the redox potential variation for $Ln^{III/IV}$ versus the atomic number [4,10].

In YF_3:(Dy^{3+},O^{2-}), the $O^{2-} \rightarrow Dy^{3+}$ CT band is located close to the bands corresponding to the $4f^n \rightarrow 4f^{n-1}5d$ transitions whose intensities do not vanish at low temperature. Then, the determination of the energy of the CT band should be much more difficult in this case without the help of Jørgensen's calculation

TABLE 1. Energy of the maximum of the CT band, observed and calculated with Jørgensen's formula, in YF_3: (Ln^{3+}, O^{2-}), and LaF_3: (Ln^{3+}, O^{2-})

	YF_3		LaF_3	
	Calculated (cm^{-1})	Observed (cm^{-1})	Calculated (cm^{-1})	Observed (cm^{-1})
Eu^{3+}	42100	42100	37500	37400
Tb^{3+}	68100		63500	
Dy^{3+}	60100	59100	55500	55500
Er^{3+}	61000	61200	56400	56400

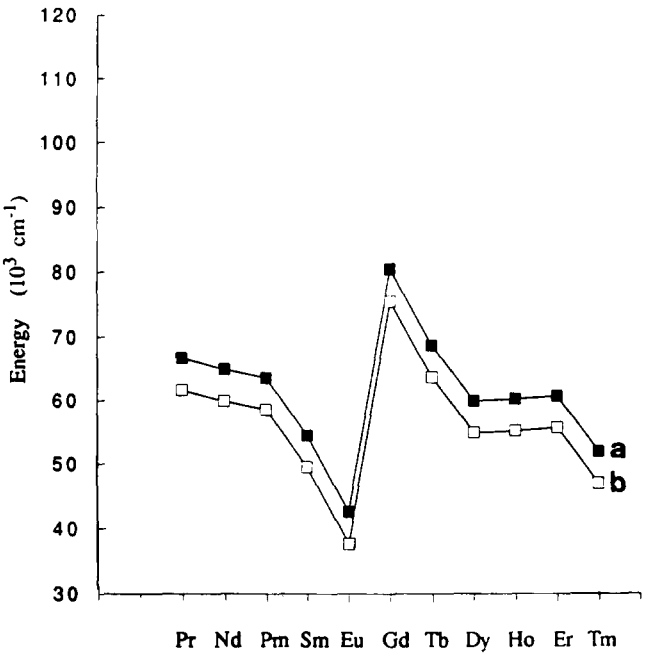

Fig. 7. Energy variation of the maximum of $O^{2-} \rightarrow Ln^{3+}$ charge transfer band in (a) YF_3:(Ln^{3+},O^{2-}) and in (b) LaF_3:(Ln^{3+},O^{2-}) calculated using Jorgensen's refined spin-pairing energy theory.

which confirms the attribution of CT to the band situated around 7.3 eV (~170 nm).

5. Charge transfer $F^- \rightarrow Ln^{3+}$

The electron transfer energy between the fluoride ligand and Ln^{3+} ion should be approximately 25×10^3 cm^{-1} higher than in oxides [20]. For the $F^- \rightarrow Eu^{3+}$ CT band, the maximum of the excitation appears clearly in YF_3:(Eu^{3+},O^{2-}) and LaF_3:(Eu^{3+},O^{2-}) at 7.9 eV (63.6×10^3 cm^{-1}) and 7.5 eV (60.5×10^3 cm^{-1}), respectively. For the other Ln^{3+} ions, the CT band $F^- \rightarrow Ln^{3+}$ is not observed.

Jørgensen has formulated another useful expression to estimate the CT band position [6]:

$$\sigma = [\chi_{opt}(X) - \chi_{uncorr}(M)]30 \times 10^3 \text{ cm}^{-1} \quad (2)$$

where σ corresponds to the energy of the CT band (in 10^3 cm^{-1}), $\chi_{opt}(X)$ is the optical electronegativity of the anion, which is approximately the Pauling electronegativity. $\chi_{uncorr}(M)$ is the optical electronegativity of the central cation.

$\chi_{uncorr}(Ln)$ was determined by using eqn. (2) with $\chi_{opt}(O) = 3.2$ [21], and $O^{2-} \rightarrow Ln^{3+}$ experimentally determined CT energies. Therefore, with $\chi_{opt}(F) = 3.9$ [6], the $F^- \rightarrow Ln^{3+}$ CT energies can be predicted in YF_3 and LaF_3 host lattices. The results are presented in Table 2. Blasse has estimated the $F^- \rightarrow Eu^{3+}$ CT band to occur in the energy range 7.45–8.1 eV ($60–65 \times 10^3$ cm^{-1}) [7]. This value is in good agreement

TABLE 2. Energy of the maximum of the charge transfer band $L^- \rightarrow Ln^{3+}$ in YF_3: (Ln^{3+}, O^{2-}) and LaF_3: (Ln^{3+}, O^{2-}) (in 10^3 cm^{-1})

	YF_3: (Ln^{3+}, O^{2-})		LaF_3: (Ln^{3+}, O^{2-})	
	$O^{2-} \rightarrow Ln^{3+}$ Experimental value	$F^- \rightarrow Ln^{3+}$ Value derived from Jørgensen's formula (2)	$O^{2-} \rightarrow Ln^{3+}$ Experimental value	$F^- \rightarrow Ln^{3+}$ Value derived from Jørgensen's formula (2)
Eu^{3+}	42.1	63.0 (63.5)[a]	37.4	58.4 (60.5)[a]
Dy^{3+}	59.1	80.1	55.5	76.5
Er^{3+}	61.2	82.2	56.4	77.4

[a]Experimental value.

with our experimental data although the calculated value of $F^- \rightarrow Eu^{3+}$ CT band for lanthanum fluoride (58.4×10^3 cm^{-1}) is slightly lower than the measured value (60.5×10^3 cm^{-1}). This difference is certainly due to misestimation of the maximum of the $O^{2-} \rightarrow Eu^{3+}$ CT band used to determine $\chi_{uncorr}(Eu)$.

$F^- \rightarrow Dy^{3+}$ and $F^- \rightarrow Er^{3+}$ CT bands have to be located at higher energy, between 75×10^3 cm^{-1} and 83×10^3 cm^{-1} (133 nm and 120 nm), but they do not show on excitation spectra recorded in this energy range at low temperature. Then, the de-excitation process involved at low temperature does not proceed *via* the population of the $4f^n$ emitting level. On excitation spectra recorded at room temperature, peaks due to $4f^n \rightarrow 4f^{n-1}5d$ transitions occur in this energy range and the CT bands are probably superposed on the f–d transitions.

The energies of the $F^- \rightarrow Ln^{3+}$ CT band estimated for Eu^{3+}, Dy^{3+} and Er^{3+} allow us to calculate the CT band energy for the other Ln^{3+} using Jørgensen's refined spin-pairing energy theory. The fit for the energy transfer $F^- \rightarrow Ln^{3+}$ in LaF_3 and in YF_3, using eqn. (1), leads to the following parameter values for W and $(E-A)$ for each system respectively:

(1) for YF_3:(Ln^{3+},O^{2-}): $W = 107.5 \times 10^3$ cm^{-1} and $(E-A) = 4 \times 10^3$ cm^{-1}

(2) for LaF_3:(Ln^{3+},O^{2-}): $W = 103.5 \times 10^3$ cm^{-1} and $(E-A) = 4 \times 10^3$ cm^{-1}

The results of these calculations are plotted in Fig. 8.

As $F^- \rightarrow Ln^{3+}$ CT occurs generally at relatively high energy, this band may be hidden by intrinsic transitions from valence band to conduction band.

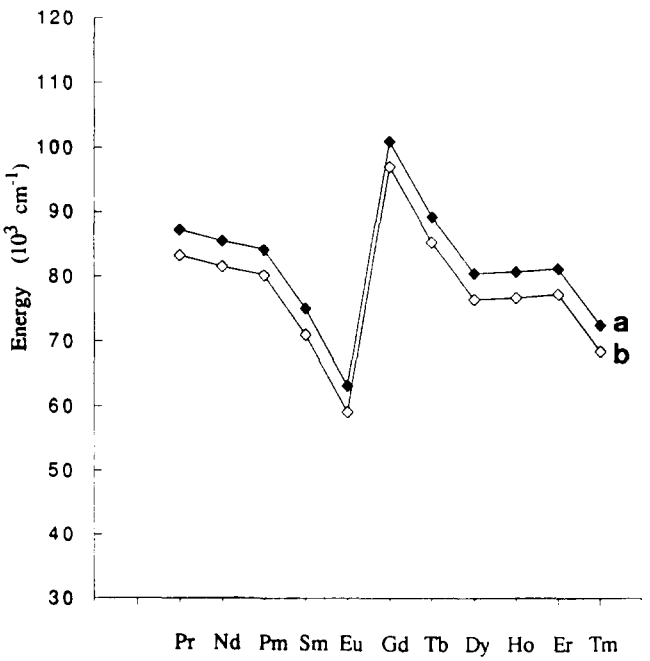

Fig. 8. Energy variation of the maximum of $F^- \rightarrow Ln^{3+}$ charge transfer band in (a) YF_3:(Ln^{3+},O^{2-}) and (b) LaF_3:(Ln^{3+},O^{2-}) calculated using Jorgensen's refined spin-pairing energy theory.

6. Profile simulation of the $O^{2-} \rightarrow Er^{3+}$ CT band in LaF_3:(Ln^{3+},O^{2-})

The configurational coordinate model, which is a picture of the effect of the lattice dynamics, is successful in explaining the shape of the broad band transitions such as CT which are generally largely vibronic in character.

Therefore the simulation of the experimental absorption profile by time-dependent theory of electronic spectroscopy, which can be treated as transitions between two potential surfaces, leads to the determination of the parameters used to establish the configurational coordinate diagram such as the Huang–Rhys parameter.

The configurational model assumes that only one lattice mode can be considered as representative of the lattice dynamics. In other words, we assume that a one-dimensional harmonic oscillator model can describe the pulsation associated with the CT state.

The time-dependent Schrödinger equation solved numerically by the method of Feit and Fleck [22] gives rise to the overlapping integrals of the vibrational eigenfunctions (φ_k at $t=0$ and $\varphi_k(t)$ at t), in the excitation state considered, using a representative harmonic potential for each level. The fundamental equation for the calculation is [23,24]

$$\langle \varphi_k | \varphi_k(t) \rangle = \exp\left\{ -\frac{\Delta_k^2}{2}(1-\exp(-i\omega_k t)) - \frac{i\omega_k t}{2} \right\} \quad (3)$$

where ω_k and Δ_k are the vibrational frequency in cm^{-1} and the Stokes shift associated with the harmonic potential of the excited state, respectively.

The Fourier transform of the overlap in the time domain leads to the absorption profile of the electronic transition induced between the fundamental and the excited states:

$$I(\omega) = C\omega \int_{-\infty}^{\infty} e^{i\omega t} \langle \varphi | \varphi(t) \rangle \, dt \quad (4)$$

where C is a constant, and $I(\omega)$ is the photon intensity, per unit volume, per unit time, at ω frequency.

The harmonic potential shape used supposes the knowledge of two parameters, the Stokes shift and the energy of the corresponding phonon associated with each level. In reverse, these parameters can be determined by fitting the experimental profile.

In the CT band case, the experimental absorption profile corresponds to a summation of numerous electronic transitions the number of which can be determined.

To fit the $O^{2-} \rightarrow Er^{3+}$ CT profile, the following hypotheses were used:

(1) each CT electronic transition is characterized by the same oscillator strength;
(2) the ground state of the 4f shell of Er^{3+} and the excited states of $O^{2-} \rightarrow Er^{3+}$ CT have representative vibrational frequencies of 390 cm^{-1} and 240 cm^{-1}, respectively, according to the phonon energies in LaF_3:Ln^{3+} measured by Schosser and Dlott [25].

The simulation performed with these hypotheses leads to eight electronic transitions and a Stokes shift corresponding to a variation in the O–Er distance of 0.7 Å. As the calculated absorption profile presented in Fig. 9 is in full agreement with the observed one, the fit corroborates the formulated hypotheses.

7. Conclusion

Oxygen traces in LaF_3 and YF_3 host lattices doped with Ln^{3+} ions give rise to $O^{2-} \rightarrow Ln^{3+}$ charge transfer in these systems which appears clearly on excitation spectra of the visible luminescence of these compounds,

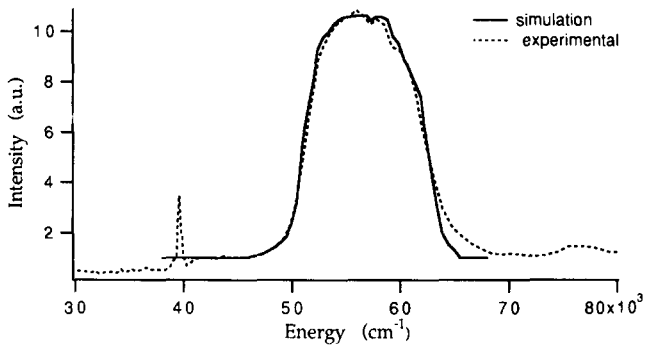

Fig. 9. Experimental and simulated $O^{2-} \rightarrow Er^{3+}$ charge transfer absorption profile.

recorded at 10 K in the VUV energy range. Determination of the energy of CT $O^{2-} \rightarrow Ln^{3+}$ for $Ln^{3+} = Eu^{3+}$, Dy^{3+} and Er^{3+} allows us to calculate the CT $O^{2-} \rightarrow Ln^{3+}$ for all the other Ln^{3+} ions of the lanthanide series, using Jørgensen's refined spin-pairing theory.

In the special case of Eu^{3+} with a $4f^6$ configuration, one electron can be added easily to reach the more stable $4f^7$ configuration corresponding to the half-filled shell. Thus, CT band $F^- \rightarrow Eu^{3+}$ is clearly observed at relatively low energy: 63.5×10^3 cm^{-1} for YF_3:(Eu^{3+},O^{2-}) and 60.5×10^3 cm^{-1} for LaF_3:(Eu^{3+},O^{2-}). Using these data and Jørgensen's theories, we predicted CT energy $F^- \rightarrow Ln^{3+}$ for each trivalent ions of the lanthanide series. The determination of the energy of this band is not a trivial problem because in fluorides, most of the CT processes arise at high energy and may overlap with two absorption mechanisms, f–d and band to band transitions.

The time-dependent theory has led to the simulation of the absorption profile of the CT band and then to the determination of the Stokes shift, phonon energy and number of electronic transitions associated with the CT band.

References

1 C.K. Jørgensen, *Mol. Phys., 5* (1962) 271.
2 C.K. Jørgensen, *Orbitals in Atoms and Molecules*, Academic Press, New York, 1962.
3 J.C. Barnes and H. Pincott, *J. Chem. Soc., A* (1966) 842.
4 L.J. Nugent, R.D. Baybarz, J.L. Burnett and J.L. Ryan, *J. Inorg. Nucl. Chem., 33* (1971) 2503.
5 H.E. Hoefdraad, *J. Solid State Chem., 15* (1975) 175.
6 C.K. Jorgensen, *Modern Aspects of Ligand-Field Theory*, North-Holland, Amsterdam, 1971.
7 G. Blasse, *J. Phys. Chem. Solids, 50* (1989) 99.
8 R. Reisfeld, *Structure and Bonding*, Vol. 13, Springer, Berlin, 1973, p. 53.
9 J.C. Barnes and P. Day, *J. Chem. Soc.*, (1964) 3889.
10 A. Garcia, R. Ibañez and C. Fouassier, *Proc. Intern. Symp. Rare Earth Spectroscopy*, Wroclaw, Poland, 1984, World Scientific, Singapore, 1984, p. 412.

11 G. Blasse, *J. Chem. Phys., 45* (1966) 2356.
12 C.G. Olson, M. Piacentini and D.W. Lynch, *Phys. Rev. B, 18* (1978) 5740.
13 I. Gérard, Thèse de l'Université de Paris Xl, 1993.
14 K.H. Yang and J.A. Deluca, *Phys. Rev. B, 17* (11) (1978) 4246.
15 J.C. Krupa, I. Gérard and P. Martin, *J. Alloys Comp., 188* (1992) 77.
16 R. Seedorf, H.J. Eichler, H. Koch, *Appl. Opt., 24* (1985) 1335.
17 A. Garcia, Thèse d'Etat, 1984.
18 L.J. Nugent, R.D. Baybarz and J.L. Burnett, *J. Phys. Chem., 73* (1969) 1177.
19 W.T. Carnall, G.L. Goodman, K. Rajnak and R.S. Rana, ANL-88-8 Report, 1988.
20 E. Loh, *Phys. Rev., 147* (1966) 332.
21 N. van Vugt, T. Wigmans and G. Blasse, *J. Inorg. Nucl. Chem., 35* (1973) 2602.
22 M.D. Feit, J.A. Fleck and A. Steiger, *J. Comp. Phys., 47* (1982) 412.
23 E.J. Heller, *J. Chem. Phys., 68* (1978) 2066.
24 E.J. Heller, *Acc. Chem. Res., 14* (1981) 368.
25 C.L. Schosser and D.D. Dlott, *Phys. Rev. B, 30* (1984) 2149.